LCLS-II BUNCH COMPRESSOR STUDY: 5-BEND CHICANE*

D.Z. Khan#, T.O. Raubenheimer, SLAC, Menlo Park, CA 94025, USA

U.S. DEPARTMENT OF ENERGY Office of Science

FEL2014

SLAC NATIONAL ACCELERATOR LABORATORY

ABSTRACT

In this paper, we present a potential design for a bunch compressor consisting of 5 bend magnets which is designed to compensate the transverse emittance growth due to Coherent Synchrotron Radiation (CSR). A specific implementation for the second bunch compressor in the LCLS-II is considered. The design has been optimized using the particle tracking code, ELEGANT. Comparisons of the 5-bend chicane's performance with that of a symmetric 4-bend chicane is shown for various compression ratios and bunch charges. Additionally, a one-dimensional, longitudinal CSR model for the 5-bend design is developed and its accuracy compared against ELEGANT simulations.

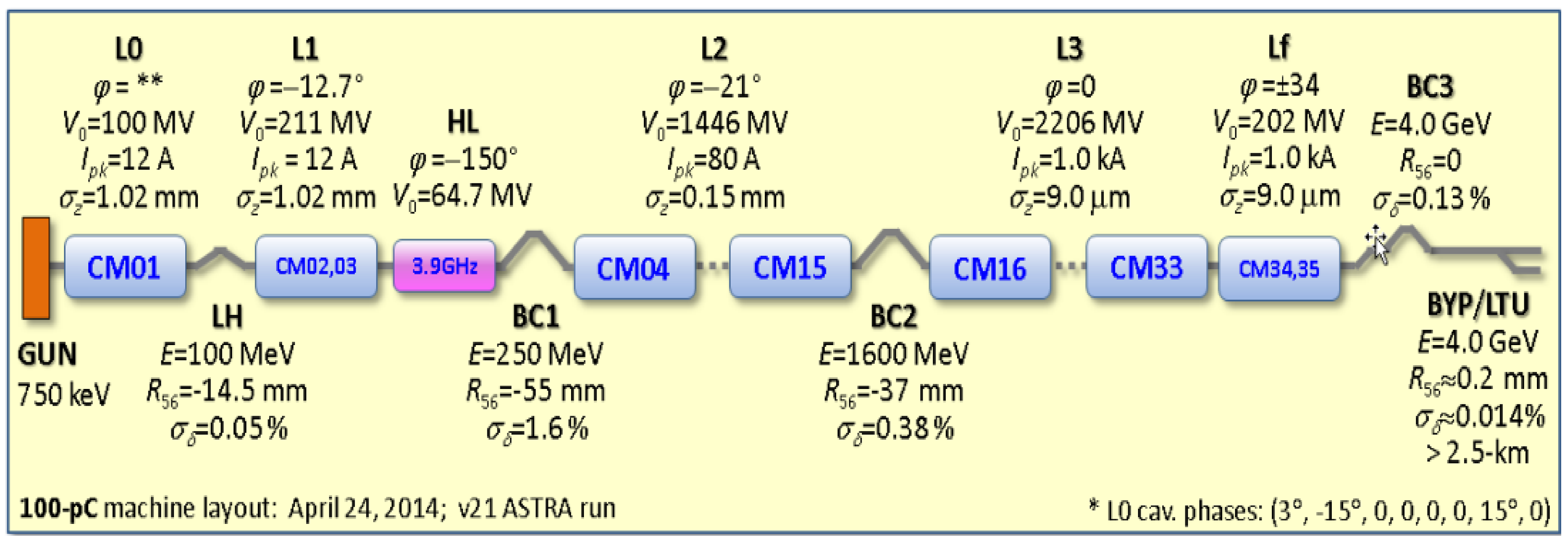

Fig. 1: A diagram of the LCLS-II beamline with relevant component details. LCLS-II plans to utilizes a two-stage magnetic chicane compression system; BC1 and BC2.

LCLS-II CURRENT BUNCH COMPRESSOR

The currently planned compression scheme of LCLS-II consists of a two-stage magnetic chicane system. Each compressor is comprised of the standard 4-bend chicane.

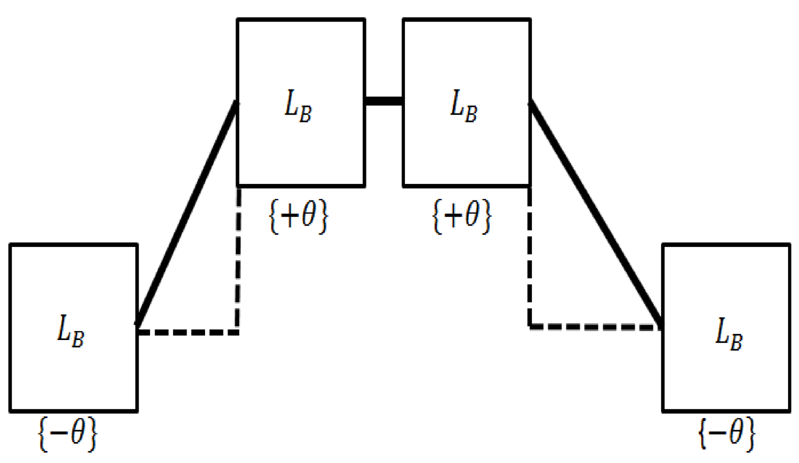

Fig. 2: Standard 4-bend chicane.

Parameter	Symbol	4-Bend Chicane
Electron Energy	E_0	1.6 GeV
Momentum Compaction	$\lvert R_{56}\rvert$	59.9 mm
Chicane Total Length	L_T	23.0 m
First Chicane Drift Length	L_D	9.8 m
Bend Angle 1	$\lvert\theta_1\rvert$	0.05 rad
Eff. Length Of Magnet 1	L_B	0.54 m
Dispersion After Magnet 2	$\lvert\eta_x\rvert$	562 mm

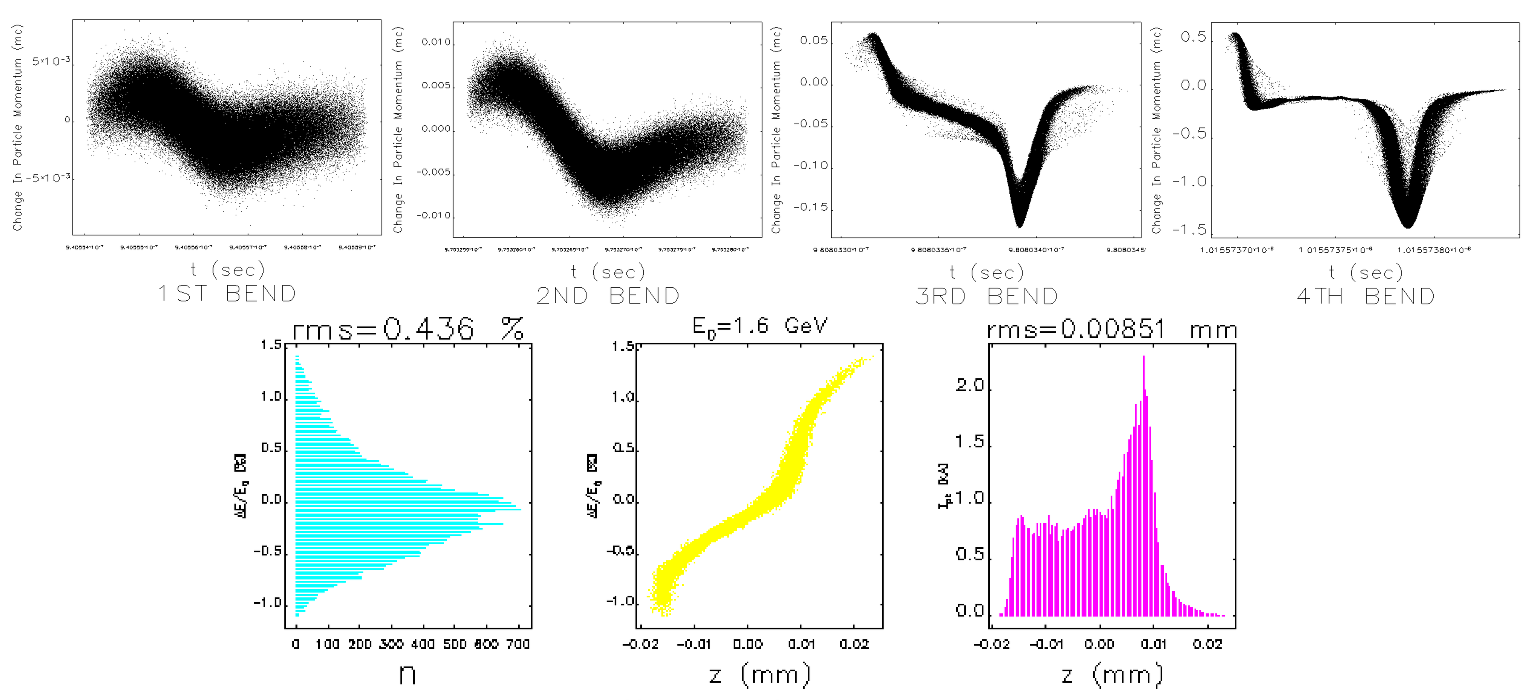

Fig. 3: Top/Middle: The momentum difference for each particle in each bend in the planned LCLS-II BC2 4-bend chicane generated with ELEGANT. The CSR wake begins to take form in the third bend where the bunch is compressed to 7 microns. Bottom: (From left to right) The normalized energy spread, longitudinal energy phase space, and the current profile of the beam at the exit of BC2.

5-BEND CHICANE

To conceptually design a chicane that completely nullifies any emittance dilution, we introduce asymmetry and an extra bend to the standard 4-bend chicane.

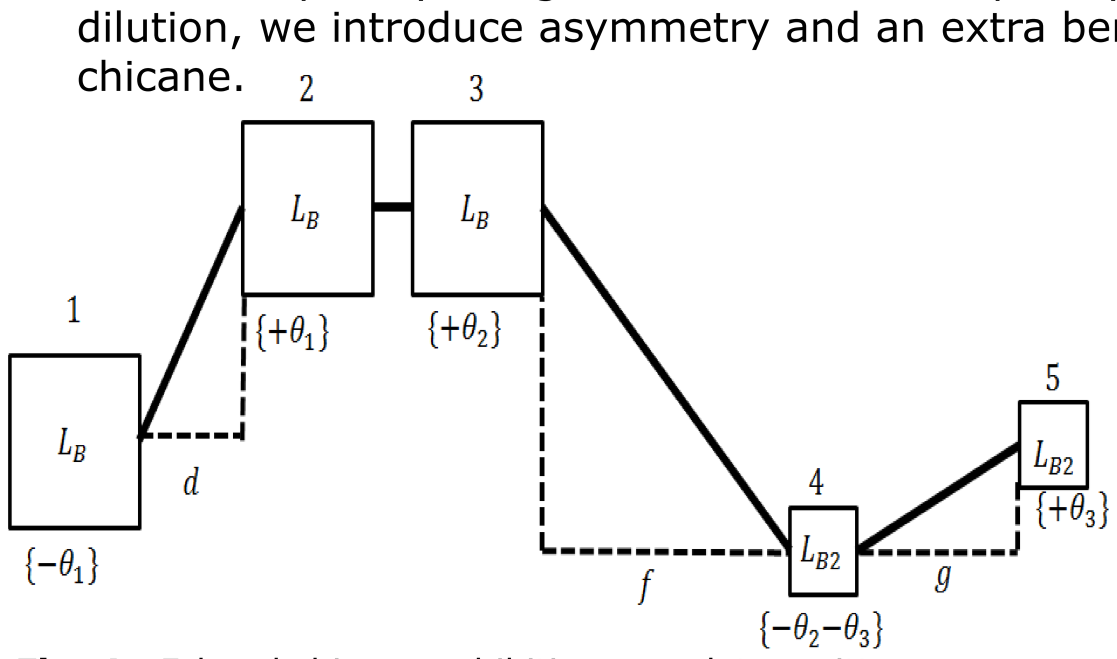

Fig. 4: 5-bend chicane exhibiting complete emittance growth cancellation.

Parameter	Symbol	5-Bend Chicane
Energy	E_0	1.6 GeV
Momentum Compaction	$\lvert R_{56}\rvert$	59.9 mm
Chicane Total Length	L_T	17.0 m
First Drift Length	L_D	3.3 m
Second Drift Length	L_F	8.7 m
Third Drift Length	L_G	1.7 m
Bend Angle 1	$\lvert\theta_1\rvert$	0.103 rad
Bend Angle 2	$\lvert\theta_2\rvert$	0.046 rad
Bend Angle 3	$\lvert\theta_3\rvert$	0.014 rad
Magnet 1 Length	L_B	0.54 m
Magnet 2 Length	L_{B2}	0.25 m
Dispersion After Magnet 2	$\lvert\eta_x\rvert$	401mm
Dispersion After Magnet 4	$\lvert\eta_x\rvert$	25 mm

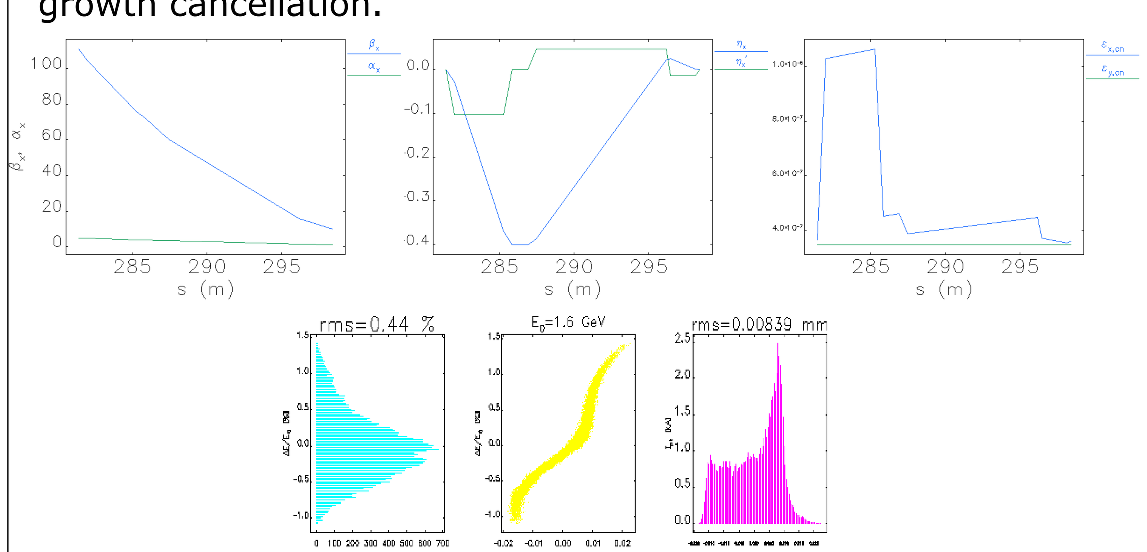

Fig. 5 (Left to right): For the 5-bend chicane: The transverse x-plane β and α functions, dispersion and slope of dispersion, corrected normalized transverse emittance (ecnx, ecny), normalized energy spread, longitudinal energy phase space, and the current profile.

DESIGN IMPLEMENTATION & ENGINEERING CONSIDERATION

Although the benefits of the 5-bend chicane is clearly evident, its complexity does provide some difficulties in actually engineering the design. We have revised the design with the following:

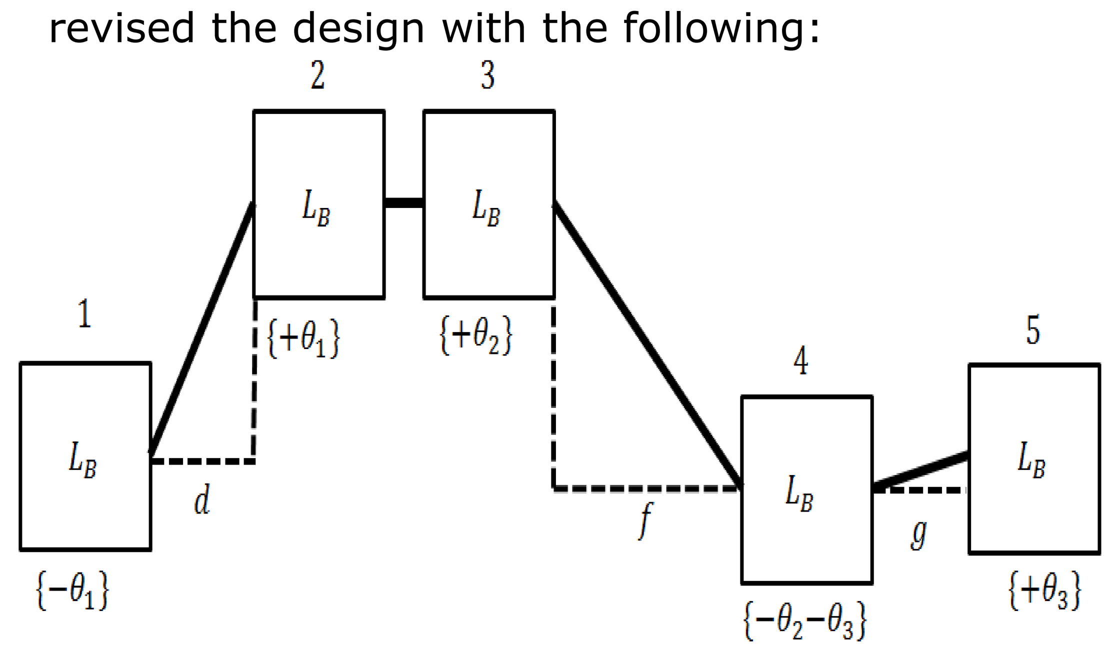

Fig. 6: Revised 5-bend chicane exhibiting highly optimized emittance preservation.

Parameter	Symbol	5-Bend Chicane
Energy	E_0	1.6 GeV
Momentum Compaction	$\lvert R_{56}\rvert$	59.9 mm
Chicane Total Length	L_T	17.8 m
First Drift Length	L_D	4.4 m
Second Drift Length	L_F	9.4 m
Third Drift Length	L_G	1.3 m
Bend Angle 1	$\lvert\theta_1\rvert$	0.087 rad
Bend Angle 2	$\lvert\theta_2\rvert$	0.046 rad
Bend Angle 3	$\lvert\theta_3\rvert$	0.014 rad
Magnet 1 Length	L_B	0.54 m
Magnet 2 Length	L_{B2}	0.25 m
Dispersion After Magnet 2	$\lvert\eta_x\rvert$	445 mm
Dispersion After Magnet 4	$\lvert\eta_x\rvert$	22 mm

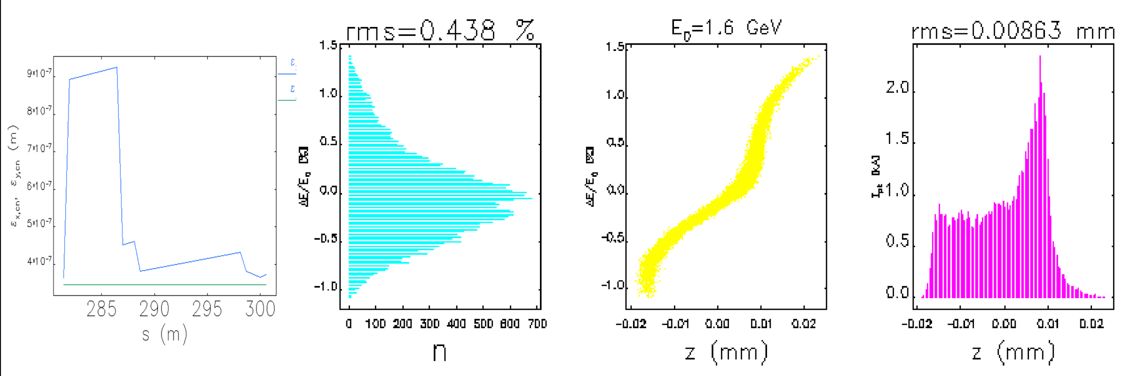

Fig. 7 (Left to right): The corrected transverse emittance (ecnx, ecny), normalized energy spread, longitudinal energy phase space, and the current profile for the revised 5-bend chicane.

5-BEND PERFORMANCE EVALUATION

For a comprehensive performance evaluation of the revised 5-bend chicane we compared its performance with that of the currently planned 4-bend chicane for two common bunch distributions and various compression ratios. The results are displayed in the tables below. The revised 5-bend chicane clearly outperforms the 4-bend chicane in emittance preservation for all cases.

"1.5kA" Chicane test of BC2 in LCLS-II

Momentum Compaction $\lvert R_{56}\rvert$ (mm)	Final Bunch Length (μm)	4-Bend ϵ_x Growth (%)	5-Bend ϵ_x Growth (%)
45.3	5.5	239	8
45.1	6.5	171	5
44.9	7.5	113	3
44.7	8.5	71	3
44.5	9.5	45	2

"1.0kA" Chicane test of BC2 in LCLS-II

Momentum Compaction $\lvert R_{56}\rvert$ (mm)	Final Bunch Length (μm)	4-Bend ϵ_x Growth (%)	5-Bend ϵ_x Growth (%)
36.6	5.5	178	23
36.3	6.5	135	13
36.0	7.5	91	8
35.7	8.5	59	5
35.4	9.5	37	4

LINEAR CSR MODEL

We developed a numerical treatment of the linear kick model for the emittance dilution cancelling 5- bend chicane, and test its results with that of ELEGANT. We have included the effects of bunch compression by approximating the bunch length as a linear function of angle traversed through the bending magnets :

$$\sigma_z(\theta) \rightarrow \frac{\sigma_{zbeg}-\sigma_{zend}}{\theta_B}\theta + \sigma_{zbeg}$$

On the treatment of the CSR self-interaction in the system we used two methods:

Steady State Regime

The CSR self-interaction is considered to be constant throughout the bunch's trajectory in the magnet (the slippage length approaches infinity) and we can calculate the RMS spatial and angular kicks by:

$$< \Delta x_i >= \int R_{16i}(s)\, \delta_{RMS-i} ds$$
$$< \Delta x_i^2 >= \left(\int R_{16i}(s)\, \delta_{RMS-i} ds\right)^2$$

$$< \Delta x'_i >= \int R_{26i}(s)\, \delta_{RMS-i} ds$$
$$< \Delta x'^2_i >= \left(\int R_{26i}(s)\, \delta_{RMS-i} ds\right)^2$$

Transient State Regime

We account for the transient effects of the CSR self-interaction as the beam is entering the magnet:

$$\frac{dE}{ds}(z,\phi) = -\frac{4}{R\phi}\lambda(z-S_L) + \frac{4}{R\phi}\lambda(z-4S_L) - \frac{2}{(3R^2)^{\frac{1}{3}}}\int \frac{d}{dz'}[\lambda(z')]\left(\frac{1}{(z-z')^{\frac{1}{3}}}\right)dz'$$

And exiting the magnet:

$$\frac{dE}{ds}(z,x,\psi) = \frac{4}{R}\frac{\lambda\left(z-\frac{R\phi_M^3}{24}\left[\frac{\phi_M+4x}{\phi_M+x}\right]\right)}{\phi_M+2x} + \frac{4}{R}\left[\int \frac{d}{dz'}[\lambda(z)]\left(\frac{1}{\psi+2x}\right)dz'\right]$$

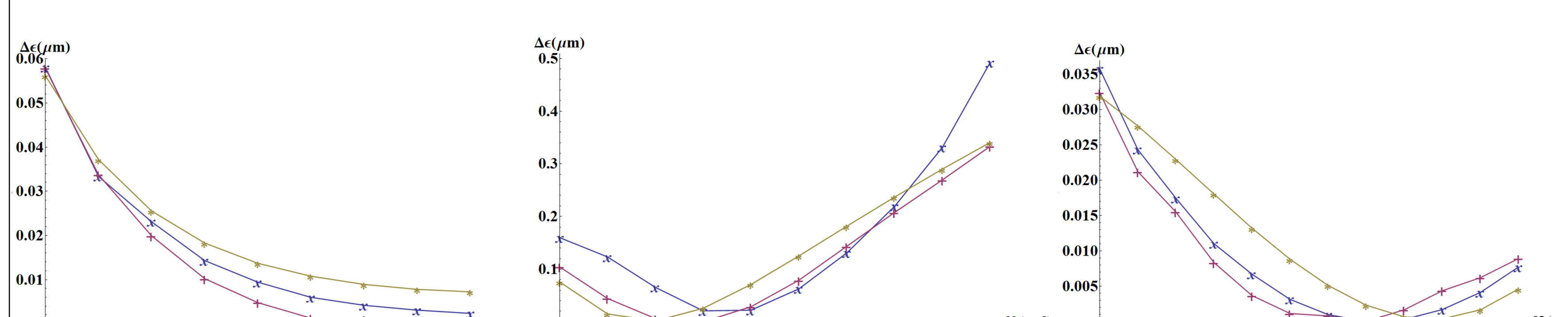

Fig. 8: Plots of change in emittance at the exit of the 5-bend chicane for various bend angle scans. For each plot, the "+" is data collected with ELEGANT, the "*" is numerical data using the steady-state linear model, and the "x" is numerical data using the transient-state linear model. Left: Displays the emittance change at the exit of the 5-bend chicane while scanning θ_1. Middle: Displays the emittance change at the exit of the 5-bend chicane while scanning θ_2. Right: Displays the emittance change at the exit of the 5-bend chicane while scanning θ_3.

*Work supported by Department of Energy Contract No. DE-AC02-76SF00515
#donish@SLAC.stanford.edu

THP027